ELSEVIER

Marine Geology 218 (2005) 113–134

MARINE GEOLOGY
INTERNATIONAL JOURNAL OF MARINE GEOLOGY, GEOCHEMISTRY AND GEOPHYSICS

www.elsevier.com/locate/margeo

RIPEX: Observations of a rip current system

Jamie H. MacMahan[a,*], Ed B. Thornton[a], Tim P. Stanton[a], Ad J.H.M. Reniers[b]

[a]*Naval Postgraduate School, Oceanography Department, Monterey, CA 93943, USA*
[b]*Civil Engineering and Geosciences, Delft University of Technology, Delft, The Netherlands*

Received 10 June 2004; received in revised form 23 February 2005; accepted 14 March 2005

Abstract

Rip current kinematics and beach morphodynamics were measured for 44 days at Sand City, Monterey Bay, CA using 15 instruments composed of co-located velocity and pressure sensors, acoustic Doppler current profilers, and kinematic GPS surveys. The morphology consisted of a low-tide terrace with incised quasi-periodic rip channels, representative of transverse bars. Offshore (17 m depth) significant wave height and peak period ranged 0.20–3.0 m and 5–20 s. The mean wave direction was consistently near 0° resulting in rip channel morphology, which evolved in response to the changing wave characteristics. An inverse relationship between sediment accreting on the transverse bar and eroding in the rip channel was found. The spatial distribution of sediment is reflected in the background rip current flow field. The mean velocity magnitudes within the rip channel (transverse bars) increased offshore (onshore) with decreasing tidal elevations and increased with increasing sea-swell energy. Eulerian averaged flows were predominantly shoreward on the transverse bars and seaward within the rip channel throughout the experiment, resulting in a persistent cellular circulation, except during low wave energy. The rip current spacing to the rip channel width was less than or equal to two, which suggests that the rip currents are influenced by each other and that no two-dimensional bar return flow should be present. The vertical velocity profile on the bar indicated that the flow was predominantly shoreward. The flow field within the surf zone was depth uniform, except for significant shear occurring near the surface, owing to Stokes drift. The wave-induced transport hypothesis is evaluated.

Keywords: rip currents; morphodynamics; nearshore; surf zone; transverse bar; circulation

1. Introduction

Rip currents are generally strong shore-normal (jet-like) flows that originate within the surf zone and are directed seaward through the breakers. Rip currents typically reach speeds up to 1 m/s and some have been reported as high as 2 m/s at Palm Beach, Australia (Short, 1985). Rip currents influence the morphology

* Corresponding author.
E-mail addresses: jhmacmah@nps.edu (J.H. MacMahan), thornton@nps.edu (E.B. Thornton), stanton@nps.edu (T.P. Stanton), ad@dutcvmm.ct.tudelft.nl (A.J.H.M. Reniers).

0025-3227/$ - see front matter © 2005 Elsevier B.V. All rights reserved.
doi:10.1016/j.margeo.2005.03.019

of the shoreline and may be important for transporting fine sediments offshore (Cooke, 1970; Komar, 1971; Short, 1999). Rip currents have accounted for more than 80% of lifeguard rescues, and are the number one natural hazard in Florida, USA (Luschine, 1991; Lascody, 1998). The understanding of rip current systems is important in developing accurate forecasts for predicting "high risk" rip current events that are a public safety hazard (Luschine, 1991; Short and Hogan, 1994; Lascody, 1998; Engle et al., 2002).

Rip currents can develop from the alongshore variations in bathymetry that induce differences in wave breaking patterns and forcing, which drive a flow from the transverse bar towards the rip channels (Bowen, 1969; Dalrymple, 1978). In the laboratory, Haller et al. (2002) verified the dynamical forcing. Waves dissipated over the bar, while the waves were larger in the rip channel owing to wave-current interaction, and dissipated closer to shore. This resulted in an increased wave set-up occurring over the bar compared to the still water level within the rip channel, which drove currents alongshore that converged within the region of lower set-up (the rip channel) and formed a rip current.

There have been few field measurements of morphologic evolution and concurrent rip current hydrodynamics, owing to the difficulty in measuring bathymetry within the surf zone and deploying instruments in the rip channels, in part because of the tendency for the rip channels to migrate alongshore. Previous field observations found that the mean rip current velocities increased with decreasing tidal elevation (Shepard and Inman, 1950; Sonu, 1972; Bowman et al., 1988a,b; Aagaard et al., 1997; Brander, 1999; Brander and Short, 2000, 2001). These experiments were short in duration (few days) and focused only on measurements within the rip channels, with minimal information available on the neighboring transverse bars. In addition, high-resolution bathymetry and local offshore directional wave measurements were often not available. Laboratory studies confirmed field observations and found that rip current velocities increase with increasing wave heights and decreasing water elevation (Dronen et al., 2002; Haller et al., 2002).

The aim of this paper is to describe the morphodynamics and flow kinematics of a rip current system in the field for a beach with rip channels, which slowly evolves over the course of a 44-day experiment. This paper attempts to describe a complete rip current system in more detail than previously available. The rip currents on this beach are topographically controlled by a low-tide terrace with quasi-periodic incised rip channels, which are representative of a transverse bar beach described by the Wright and Short (1984) morphodynamic model.

2. RIPEX experiment

2.1. Instrumentation

RIP current field EXperiment (RIPEX) was performed in conjunction with a steep beach experiment during the months of April and May 2001 at the southern end of Monterey Bay in Sand City, CA. The foreshore of the beach was relatively steep (1:10) with beach cusps O (35 m), flattening out to a low-tide terrace (1:100) with quasi-periodic, O (125 m), incised rip channels, continuing with a 1:20 offshore slope, representative of a transverse barred beach by the Wright and Short (1984) morphodynamic model (Fig. 1). Feeder channels were present near the shoreline connecting to the incised rip channels. The rip channels began at the low-tide line and increased in width in a quasi-exponential fashion seawards to a depth of 4 m.

Spatial and temporal scales of rip current behavior and morphological evolution were measured using a combination of in situ co-located pressure and bi-directional electromagnetic (em) current sensors (PUV), time-lapsed video observations, and rapid deployment bathymetric surveys. The flow dynamics over the alongshore variable bathymetry were measured using an alongshore array of 6 PUVs. Additional instruments were deployed over the transverse bar and rip channels. Velocity profile measurements within the rip channel were obtained using a portable acoustic Doppler current profiler (ADCP), which has a 5 cm blanking distance and 20 cm bins (first bin is at 25 cm). Velocity profiles over the transverse bar were measured using a vertical array (MAST) of 8 em current meters, starting at 10 cm off the bed with ~40 cm spacing that spans 2.56 m. After yearday 117, the em current meters within the rip channels were oriented downward in order to obtain measurements during lower tidal

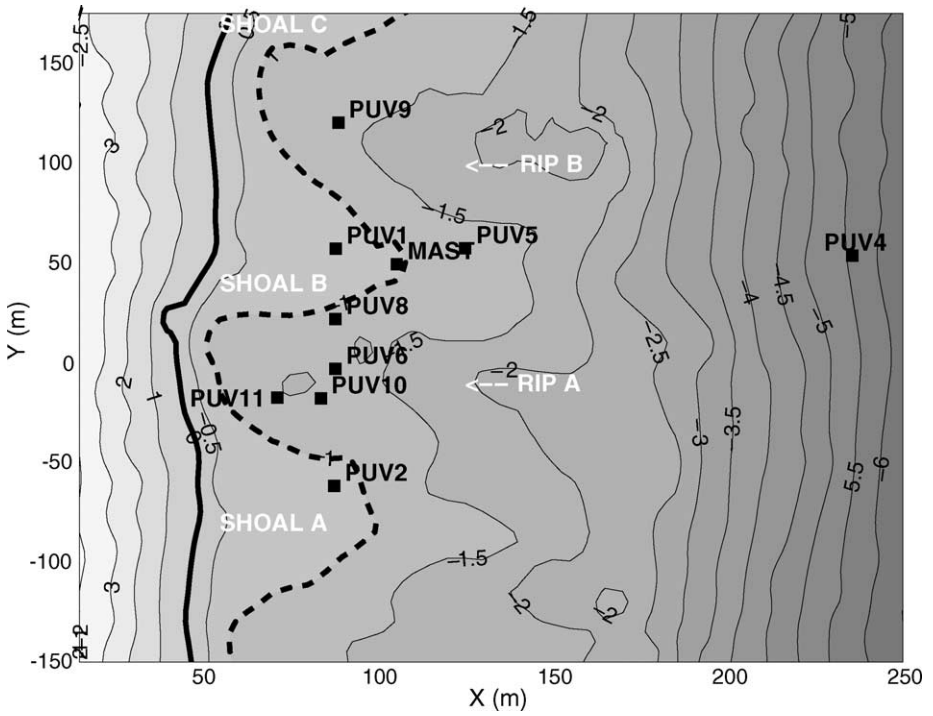

Fig. 1. Local bathymetry for yearday 117. The squares represent locations of co-located pressure and bi-directional em current meters. The MAST is a vertical array of 8 em current meters with wave sensor. The solid line is the MSL contour and the dashed line is the mean low water contour.

elevations. Current meters on the transverse bar were oriented upward and were not always submerged at low tides. The current meters were horizontally aligned with the shoreline, which did not vary over the course of the experiment owing to the waves approaching near shore-normal throughout the experiment (discussed in the next section). Cosine responses of the two-axis em current sensors have been established by repeated constant velocity calibration runs in a 6m long computer-controlled tow-tank. The sensor was rotated in 10 degree increments at both 0.1 and 1 m/s tow speeds. Results fit a true cosine speed response within 4%, which is very good for an invasive sensor. Currents are described as either cross (U)- or alongshore (V). The right-hand rule orientation was adapted, such that flows were positive seaward, to the south, and upward. All instruments were sampled synchronously and continuously at 8 Hz, except the portable ADCP, which sampled at 1 Hz.

Bathymetric surveys were performed using a differential, kinematic, global positioning system (KGPS) mounted on a sonar equipped personal watercraft, PWC (MacMahan, 2001). Plunging breakers at the outer edge of the transverse bar injected significant amounts of air bubbles into the water column, making the bar area acoustically opaque for the echosounder. At high tides, the PWC traversed from offshore (~7 m water depth) to the outer edge of the transverse bars and within the rip channels. Wave breaking was generally less within rip channel systems allowing for safe PWC operation and bathymetric surveys. At low tides, the transverse bars and feeder channels were surveyed by a walking person carrying the KGPS housed in a water-tight back-pack. The beachface and foredune were surveyed with the KGPS mounted on an all-terrain vehicle, ATV. Bathymetry is referenced to mean sea level (MSL).

2.2. Wave climate

Offshore waves were recorded by a directional wave rider buoy (DWR) located 650 m offshore in 17 m water depth and by a National Oceanographic and Atmospheric Association National Data Buoy Center

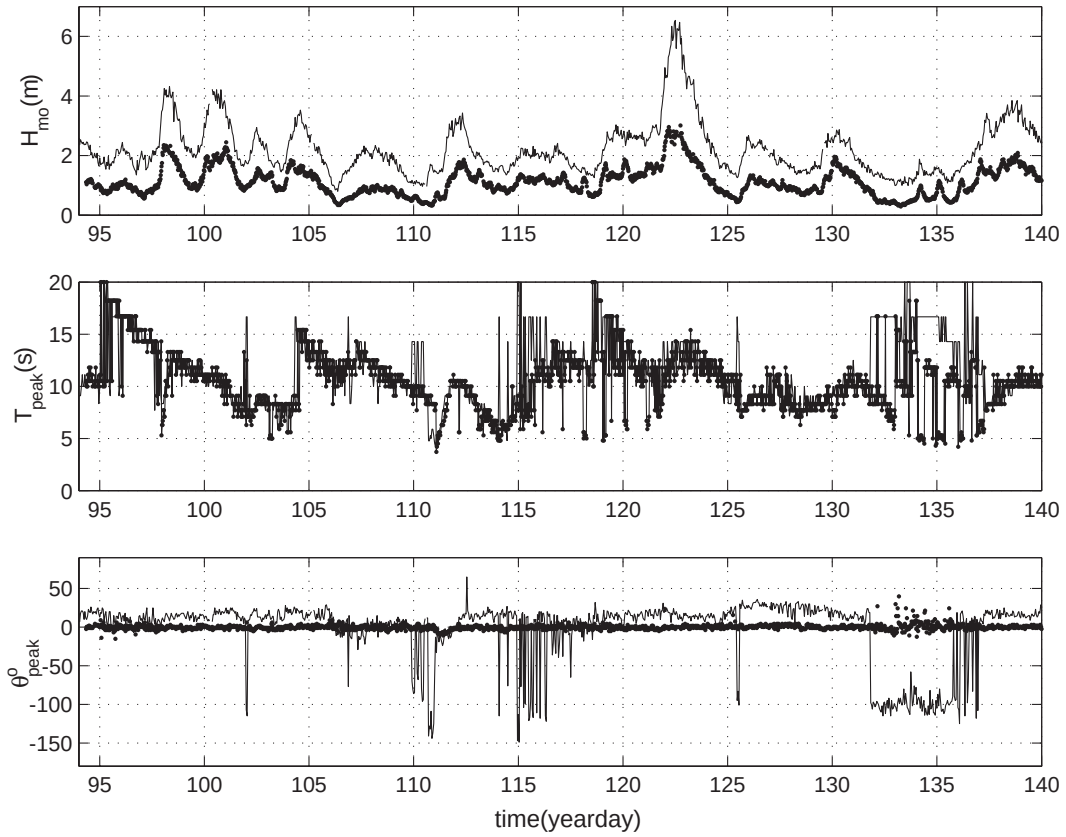

Fig. 2. (Top) significant wave height, (middle) peak wave period, and (bottom) peak wave direction relative to shore-normal measured at directional wave buoy (DWR—bold line) located 650 m offshore in 17 m water depth and the NDBC buoy #46042 located 40 km offshore of Monterey Bay, CA.

Buoy (NDBC) #46042 located 40 km offshore, outside of Monterey Bay, CA. Large variation in significant wave heights (H_{mo}), peak wave periods (T_p), and wave direction (θ_{peak}) at the peak frequency, occurred throughout the experiment (Fig. 2). The peak wave period at the two buoys were similar most of the time, which is indicative of swell conditions. Large differences in T_{peak} occurred during times of local wave generation at DWR. The decreases in H_{mo} and θ_{peak} are associated with sheltering by the local headlands and strong refraction over Monterey Canyon, which filters out most wave directions. H_{mo} and T_p at DWR ranged from 0.20–3.0 m to 5–20 s. The nearshore mean wave incidence angle shows little variation with a mean direction and standard deviation of 0° and 3° to shore-normal. Except for times of local wave generation (sea breeze events), the waves approach shore-normal, even though the variation in wave directions outside the bay (NDBC) are significantly larger. Due to the near-normal incidence of waves most of the time, long-shore currents were weak or non-existent, except for those associated with the rip current cellular circulations (Section 4).

3. Morphodynamics

Beach cusps (O (35 m)), mega-cusps (O (125 m)) and rip channels (O (125 m)) characterized the morphology of this beach system, but the governing processes controlling these features differ. Beach cusps occurred at smaller spatial scales, related to swash zone processes, while the rip channels are related to surf zone processes, which develop mega-cusps on the beachface. At smaller-scales (O (1 m)),

mega-ripples within rip channels were observed throughout the experiment similar to observations of rip channel systems by Cooke (1970), Sherman et al. (1993) and Thornton et al. (1998), but no quantitative measurements were obtained in the rip channel. On the transverse bars, a scanning-altimeter recorded migrating orbital ripples during moderate and low wave forcing and flat bed, sheet flow conditions during high wave days (Weltmer, 2003).

3.1. Beachface

Detailed beachface survey data were acquired from yeardays 114–136 along a 2 km stretch from Sand City south to Del Monte Beach, CA. Two beachface features are prominent: (1) beach cusps (O (35 m)) and (2) mega-cusps (O (125 m)) associated with the rip channel geometry (Fig. 1). The beach cusp spacing was essentially constant along the entire length of the beach, despite decreasing beach slope and wave heights to the south (Miller, 2001; Holt, 2003). The beach cusps remained stable at relatively fixed longshore wavelengths until a storm event (yearday 122) occurred, which destroyed the cusp pattern. This behavior supports previous observations of Wright et al. (1982) that once the cusp spacing has been cut into a beach, it remains until a wave event occurs that establishes a different cusp spacing (Miller, 2001). Unfortunately, only one storm event (yearday 122) occurred during the observational period (yeardays 114–136) that was large enough to modify the beach cusp spacing.

Mega-cusps had the same length scale as the rip current spacing, with the rip current located at the

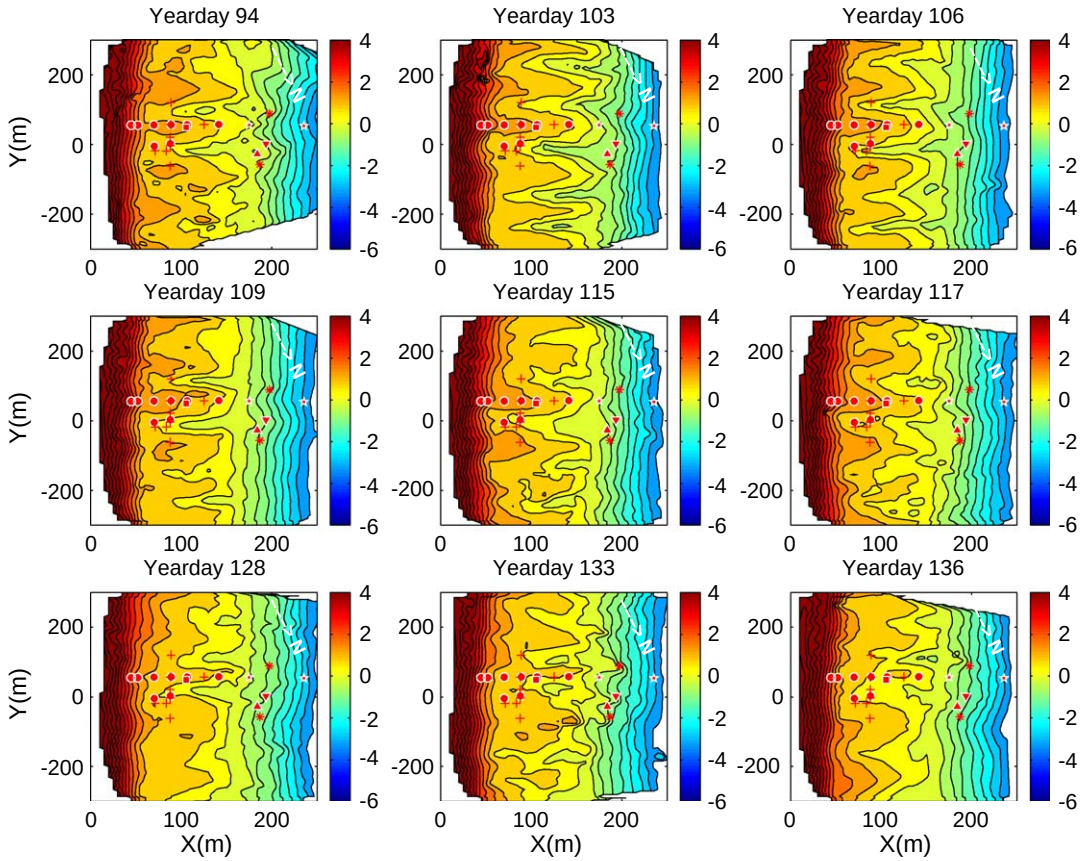

Fig. 3. Bathymetric surveys for the RIPEX experiment elevation (z(m)) color scale on the right.

center of the rip (mega-cusp) embayment. The mega-cusps were also relatively stationary throughout the experiment. Mega-cusps appear to be erosional features of rip currents owing to the fast-seaward directed flow creating an erosional embayment (Short and Hesp, 1982). As only limited measurements were available, the erosional and accretional patterns are not discussed (see Komar, 1998; Short, 1999 for more information).

3.2. Bathymetry

Bathymetric variations occurred as a result of accretion and deposition throughout the experiment. The rip channel and transverse bar geometry persisted, although features slowly migrated and varied in dimensions (Fig. 3). The nearshore morphology evolved continuously in response to 10 wave height events ($H_{mo}>1$ m). The largest storms occurred on yearday 98 and 100 ($H_{mo}>2.5$ m) and yearday 122 ($H_{mo}>2.9$ m), causing significant bathymetric variations (Fig. 3). The storms on yeardays 98 and 100 resulted in the rip channel at $y=100$ m migrating downcoast approximately 50 m (unfortunately, no nearshore hydrodynamic measurements were obtained until yearday 103).

At the beginning of the experiment, the bathymetry was well organized and rip channels and

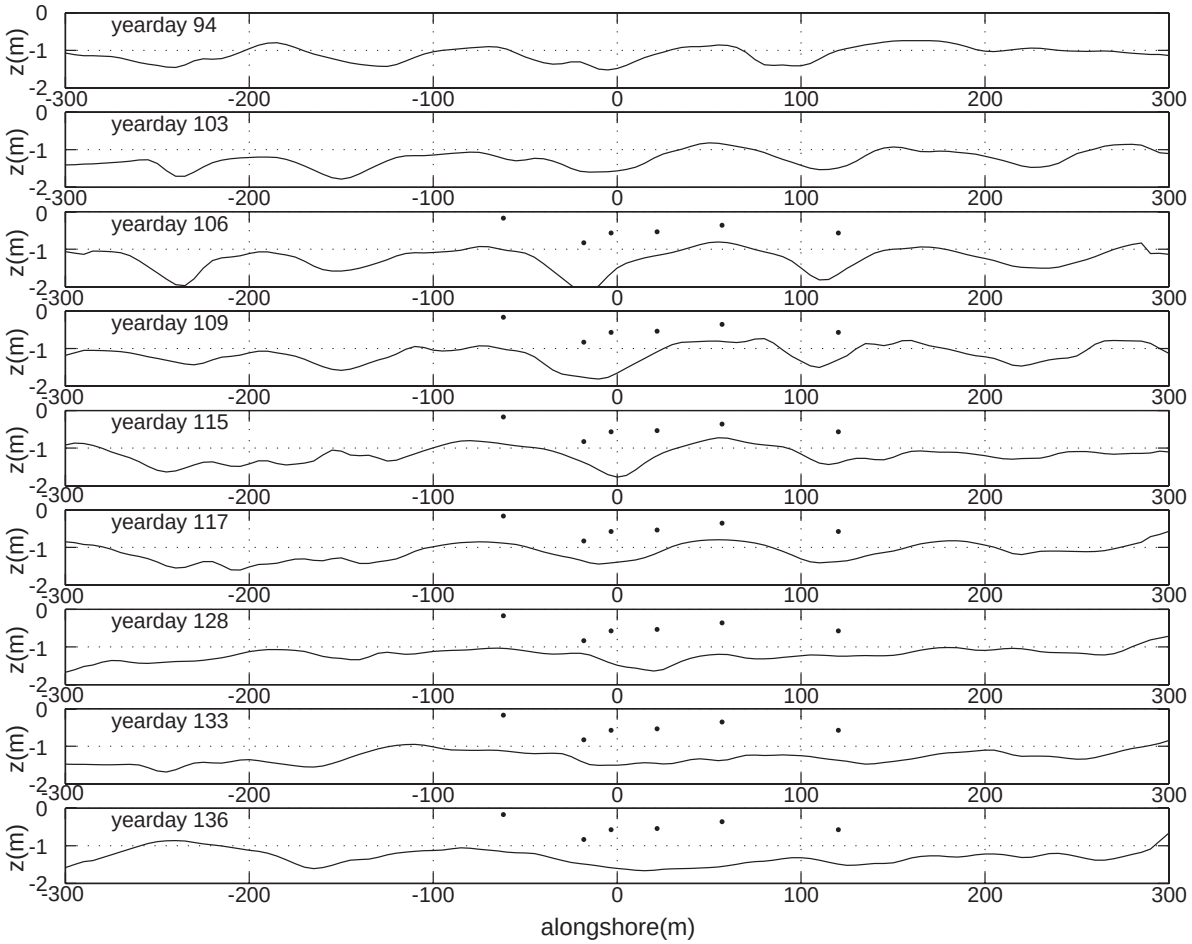

Fig. 4. Alongshore profiles at cross-distance 100 m for the various days of bathymetric surveys. Alongshore array at cross-shore distance 88 m are represented by dots.

transverse bars were clearly defined. After the storms of yeardays 98 and 100, the rip channels shifted orientation and the transverse bars began accreting until the storm of yearday 122 (Fig. 3). The storm of yearday 122 caused significant amounts of transverse bar erosion and rip channel accretion with additional random deposition and erosion (Fig. 3), except for the channels near the arrays scoured deeper. This storm decreased the bathymetric relief, reducing the alongshore depth variability associated with the rip channels and transverse bars. The rip channels were still present, but their amplitudes decreased (in the alongshore), as compared with the deeper channels at the onset of the experiment (Fig. 4). The transverse bar on which the cross-shore instrument array was located remained relatively stable throughout the experiment. However, the morphology associated with rip channels located north of the instrument array experienced significant bathymetric variations and at times no rip channels were present. Note there is a riprap wall at the shoreline around $y=-350$ m (not shown), which caused significant wave reflections at high tide, potentially influencing the rip current cells in this vicinity. The region of the riprap wall was not surveyed.

3.3. Inferred morphology from video images

Two video cameras overlooking the experiment site were mounted on a 10 m tower with its base 8.2 m above the mean water line. Images from the cameras began on yearday 118. Snap shots and 5 min time-average images were obtained every 20 min to document the morphodynamics between bathymetric surveys. Rectified time-averaged images depict variations in depth-limited wave breaking from which morphologic beach patterns can be inferred (Lippmann and Holman, 1990). The rectified time-averaged intensity images compare well with the bathymetric surveys (Fig. 5). Depth-limited wave breaking occurs on the bar outlining shallow regions, while the deeper sections of the rip channel have minimal wave breaking. An alongshore pixel intensity line was selected at the 100 m cross-shore distance and plotted as a function of time (Fig. 6), referred to as a timestack. The timestack indicates that the rip channels were

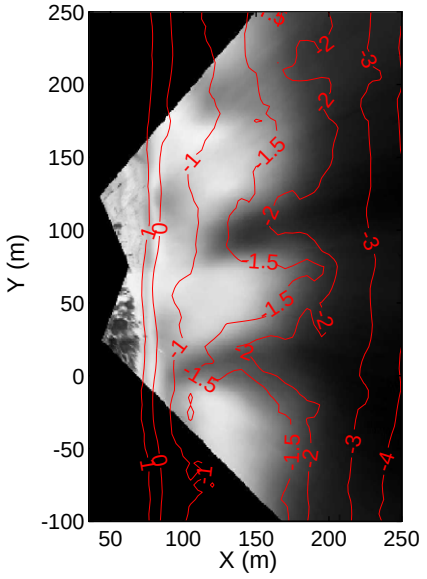

Fig. 5. Rectified time-averaged video exposure with bathymetric contours overlayed on top for yearday 128.

~30 m in width and the transverse bars were ~70 m in alongshore width before the storm of yearday 122. After the storm event of yearday 122, the rip channels became slightly wider ~40 m and the transverse bars became narrower ~60 m. However, the smaller storm event of yearday 130 had the most influence in modifying the underlying morphology, as the rip channels became wider ~60–70 m and the transverse bars became narrower ~30–40 m (in alongshore width). The video images correspond well with the alongshore profile evolution (Fig. 4), and are a good proxy for the subaqueous morphology for $H_{mo} \leq 2.0$ m, except for small wave conditions $H_{mo} \leq 0.5$ m. For larger waves, such as occurring on yearday 122, wave breaking occurs within the rip channel, obscuring the rip channels (Fig. 6).

3.4. Erosional–accretional trends

The volume of sediment on the transverse bars and within the rip channels are compared. The volume of sediment for the transverse bars was calculated between depths −1.2 m (offshore minimum tidal elevation) and MWL, which is generally higher than the transverse bars. The volume of

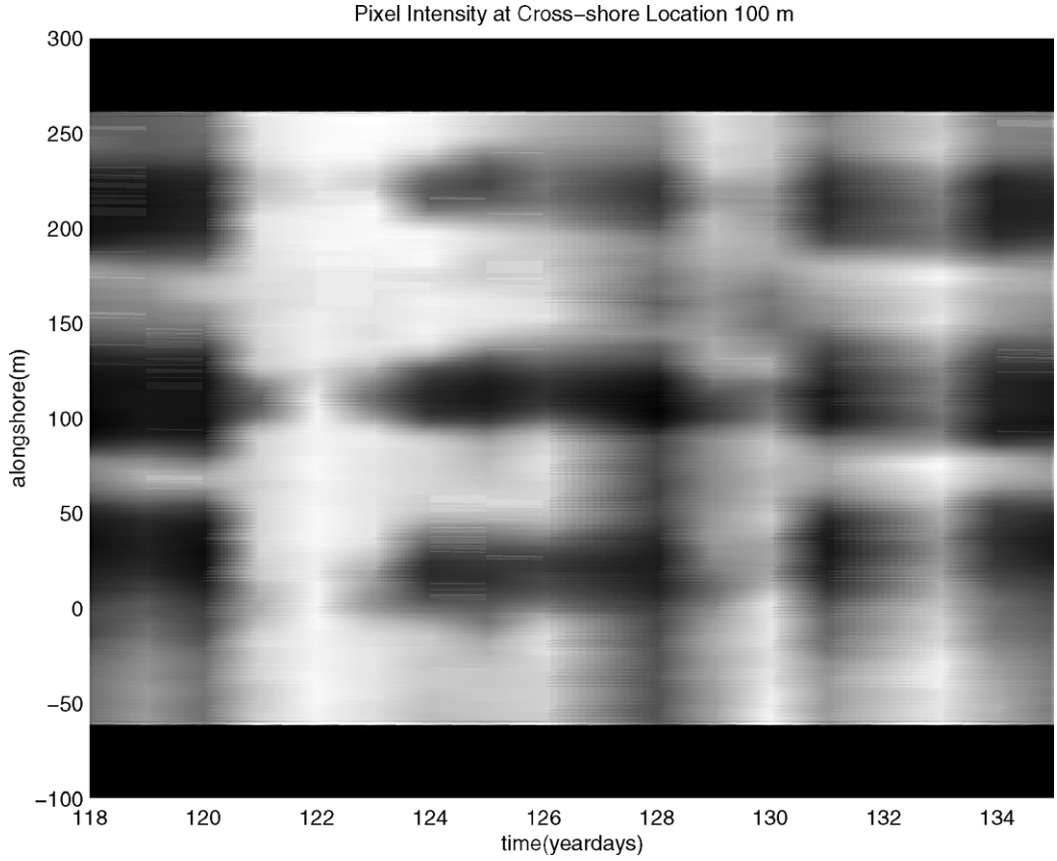

Fig. 6. Alongshore pixel timestack at the 100 m cross-shore location. Light areas indicate waves breaking on the transverse bar and dark areas indicate deeper rip channels.

sediment within the rip channels was computed between −2.4 m to −1.2 m, which encompasses the region just outside of the active surf zone. The first survey was conducted on yearday 94. After yearday 94, four relatively short storms induced a significant amount of erosion for both the transverse bars and rip channels (Fig. 7). Following the survey of yearday 106, the system began accreting around yearday 109. After yearday 109, an inverse relationship developed between erosion and accretion for the transverse bars and the rip channels. While sediments accrete on the transverse bars, they erode within the rip channels (and vice-a-versa) (Fig. 7), which is similar to observations by Brander (1999). A large storm occurred on yearday 122 (H_{mo}>2.6 m) eroding the beachface and redistributing the sediment within the sub-aqueous profile (−4 m MSL), smoothing out the alongshore variability (Figs. 3, 4 and 7).

4. Rip current flow kinematics

4.1. Cellular circulation

In general, the flow was directed shoreward on the transverse bars and seaward within the rip current channels. The measurements are consistent with a cellular circulation (Fig. 8) and more detailed laboratory experiments (Haller et al., 2002; Haas and Svendsen, 2002). The flow within the rip channel increases at low tides. Histograms of 90 min mean cross-shore and alongshore velocities were computed for the entire experiment (Figs. 9

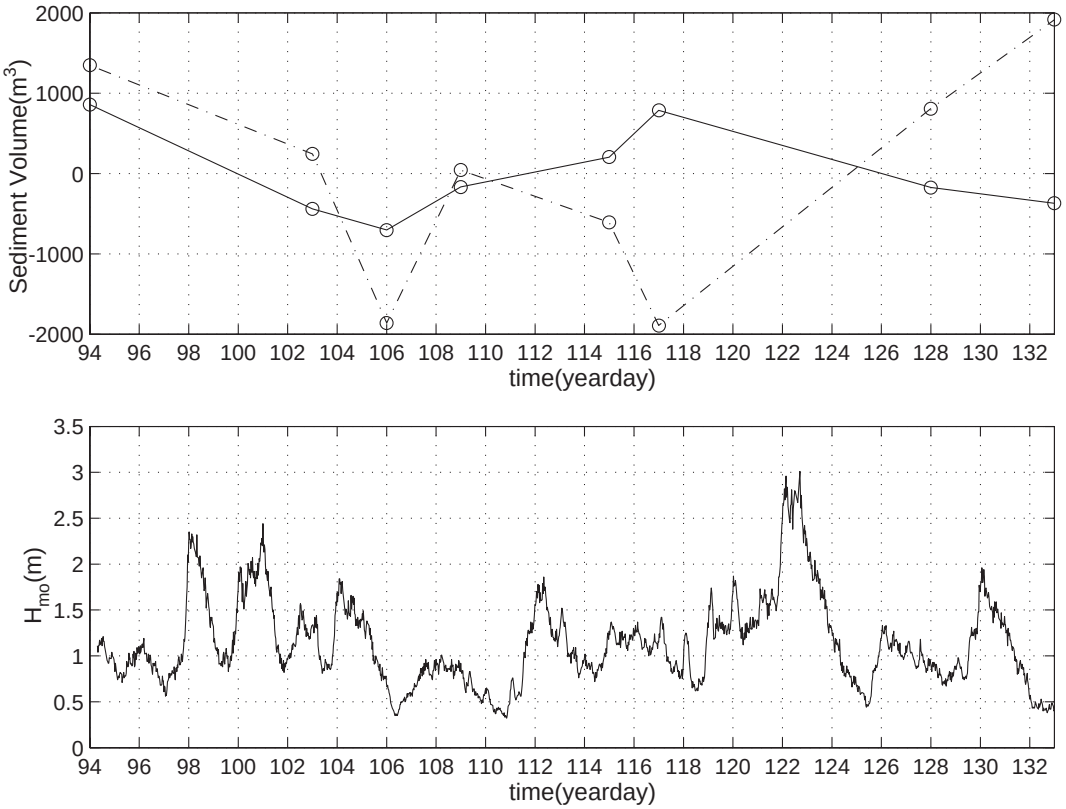

Fig. 7. (top panel) Calculated volumes for the transverse bars (solid) and the rip current channels (dashed-line). (bottom panel) H_{mo} measured at the 17 m buoy during the periods of bathymetric surveys shown as reference.

and 10). The probability of the flow directed seaward (shoreward) for measurements within the rip channel (on the transverse bar) were calculated. The cross-shore flow was predominantly shoreward ($P \simeq 0.9$) for instruments (PUV1, PUV2, PUV5) located on the transverse bar and seaward ($P \simeq 0.9$) for instruments (PUV6, PUV9, PUV10, PUV11) located within the rip channels throughout the experiment (Fig. 9). The small occurrence (~10%) of opposite flows is associated with periods of small currents. PUV11 measured shoreward flows early in the experiment, as it was on the edge of the transverse bar.

The direction of alongshore velocities, shown in Fig. 10, was relatively equally distributed for some instruments (PUV5, PUV6, PUV10) and directionally biased for other instruments, related to their location within the rip current cellular circulation (Fig. 1). The morphologic evolution induces much of the directional variability in the alongshore currents (Figs. 4 and 10).

PUV1 and PUV2, located on opposing transverse bars, show net onshore flows, though the magnitude was reduced relative to that of PUV5 (Fig. 10), located at the end of the transverse bar. The alongshore velocities at these two sensor locations preferentially flowed toward the rip channel located at $y=0$ m (RIP A—see Fig. 1), and were on the same order of magnitude as the cross-shore velocities (Fig. 9). PUV10, located within RIP A closest to the shore near the feeder channel of SHOAL A, measured velocities that were downcoast and offshore toward RIP A. Two PUV sensors (PUV6, 11), located across the rip channel (*RIP A*), measured significant offshore and alongshore velocities. PUV9, located in RIP B, had significant offshore flows similar in magnitude to PUV6 and PUV11, located in RIP A. PUV9, located within the RIP B close to SHOAL C, also had

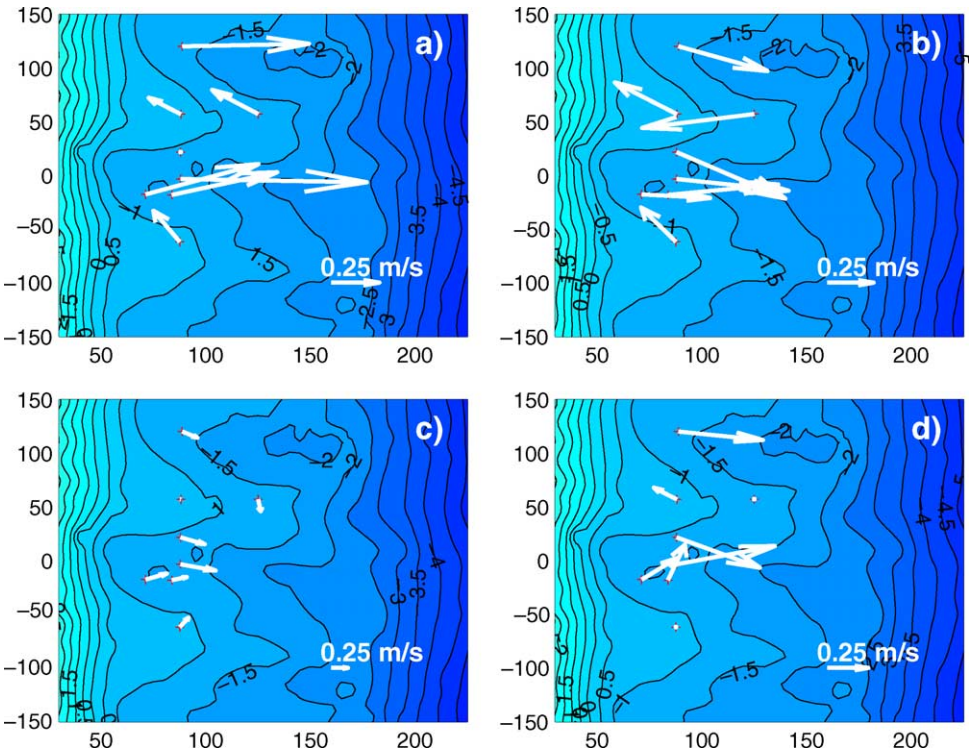

Fig. 8. Hourly mean velocity vectors for yearday 122 (top panels) and 120 (bottom panels) at high (right panels) and low tide (left panels). An instrument location without a velocity vector indicates that the em was not submerged.

alongshore flows directed toward the center of RIP B. Throughout the experiment RIP A slowly migrated downcoast, which is reflected in rip current velocities at PUV6 that initially flowed upcoast turned and flowed downcoast.

During the apex of the storm on yearday 122, PUV9 located within the southern rip channel registered maximum offshore flows of ~1 m/s, whereas PUV6 and PUV10 reached a maximum of ~1 m/s and ~0.5 m/s. The rip channels were visually apparent owing to the waves breaking on the transverse bar and not within the rip channel (Fig. 6). During the storm of yearday 122, wave heights exceeded 3 m producing significant wave breaking within the rip channel and the identification of rip channels was obscured. However, the measurements indicated that the offshore flow within the rip channels was still significant (Fig. 8).

The mean rip current velocities were O (30 cm/s) during the experiment for a wide range of wave conditions (Fig. 2), with maximum mean rip current velocities approaching 1 m/s. Rip currents have been observed to pulsate on wave group temporal scales (Shepard and Inman, 1950; Sonu, 1972; Brander and Short, 2001; MacMahan et al., 2004a,b). Infragravity rip current pulsations increase the instantaneous rip current maximum flow to over 1 m/s over a period of 25–250 s. Furthermore, the tide can also vary the flow velocity significantly over the course of a few hours. However, the overall mean flow field was typically on the O (30 cm/s).

4.2. Distribution of sediment within a rip current system

Sediment distributions are related to the morphodynamics and spatial variations in the flow field for a rip current system (Figs. 8–10). Cumulative size distributions of surface (<8 cm deep) sediment samples were determined using sieve analysis. D_{50}

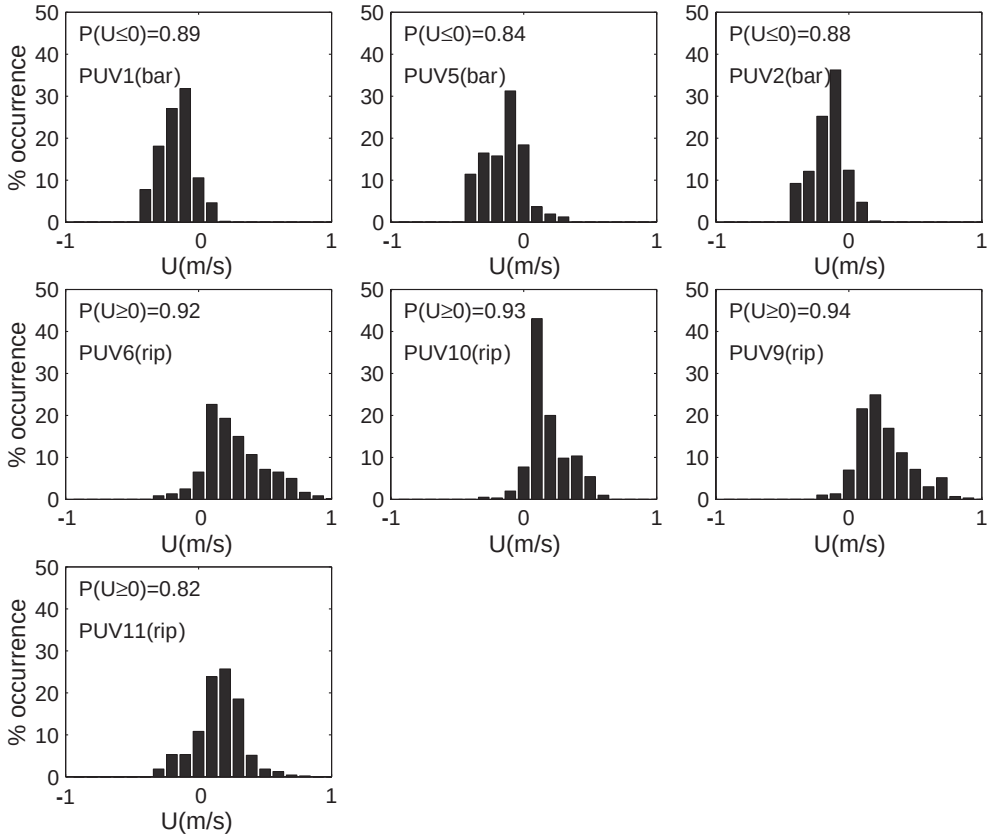

Fig. 9. Histograms of 90 min mean cross-shore velocities for yeardays 107–140. Positive U is offshore.

was linearly interpolated from the cumulative distribution. The spatial sediment distribution of D_{50} (Fig. 11) indicates that the beachface was composed of a course sediment (D_{50}: 0.66–0.72 mm), which was reflected in the steep profile. The top of the beachface, located at the toe of the foredune, had finer sediments (D_{50}: 0.47–0.54 mm) associated with wind-driven processes and erosion of the foredune. The sediment sizes were also finer (D_{50}: 0.34–0.37 mm) at the base of the beachface, where the profile became milder. The sediment sizes were reasonably uniform across the transverse bar to its outer edge (D_{50}: 0.32–0.43 mm), at which point the profile began to steepen and D_{50} increased to 0.47 mm. At the low tide swash break, there was a narrow region occupied by larger sediments (D_{50}: 0.61 mm) created by the swash backwash, located at the shoreward extent of the rip channel. Sediments were generally coarser within the rip channels (D_{50}: 0.40–0.48 mm), decreasing in size closer towards the transverse bars (D_{50}: 0.34–0.38 mm).

The spatial distribution of D_{50} can be explained by the cellular circulation associated with rip current cells, which was a persistent background flow (Fig. 8). The rip current transports sediments through the rip channel with coarser sediments deposited at the rip channel, while finer sediments are transported offshore. Owing to the cellular nature of the rip currents, the fine sediments are re-deposited on the seaward side of the transverse bars. Finer sediments are then transported onto the transverse bar. The spatial distribution of surface sediment sizes reflects the hydrodynamics of the rip morphology, consistent with Bowman et al. (1988a,b). The cellular circulation is also supported by the predominant onshore ripple migration

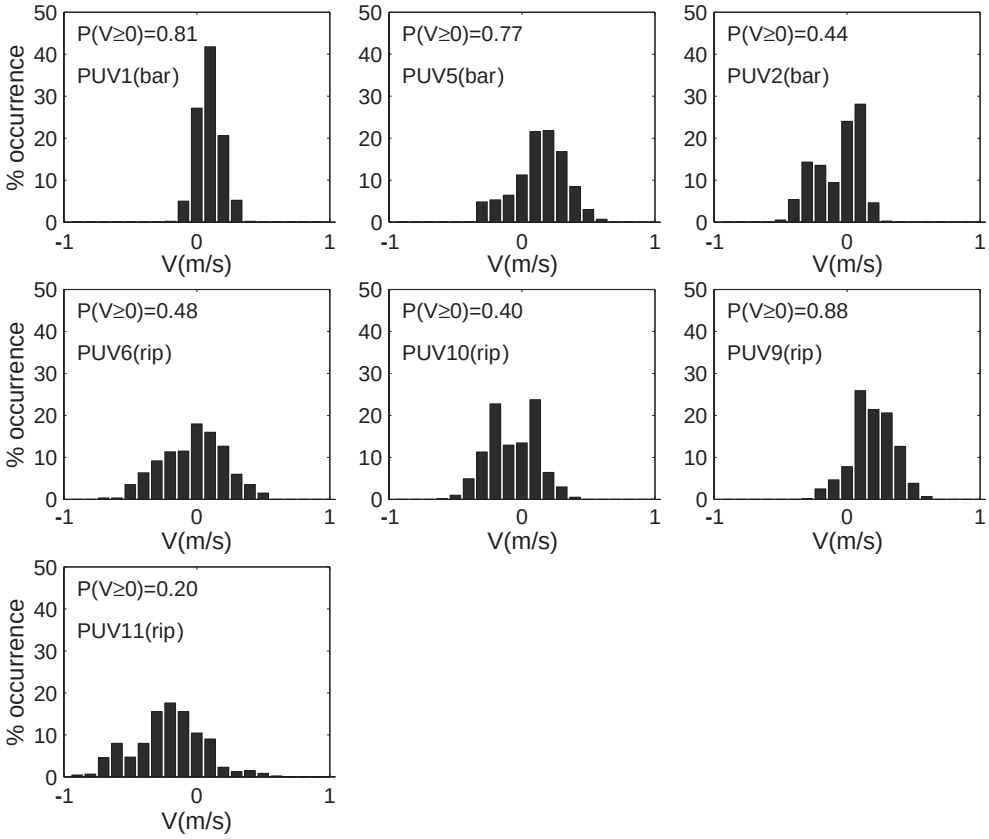

Fig. 10. Histograms of 90 min mean alongshore velocities for yeardays 107–140. Positive V is north.

observed hourly on the transverse bar near the location of the MAST (Weltmer, 2003).

4.3. Vertical velocity profiles

It has been assumed throughout that the em current meters at a single elevation represents the depth-averaged flow of the cellular circulation within the surf zone. A vertical em current meter array (Fig. 1—referred to as MAST) and a portable vertical profiling ADCP are used to evaluate this assumption. The portable ACDP was deployed within the rip channel at various times throughout the experiment. The single point em current meters were located approximately 25–30 cm off the sea bed, similar to the first bin of the ADCP. The mean minimum depth of water for all of the ADCP deployments was 1.25 m at low tide. The first bin of the ADCP was approximately 25 cm off of the bed. The lowest em current meter for the tower was approximately 10 cm off of the bed, which is influenced by the bottom boundary layer. Velocity profiles were time-averaged (60 min) and depth-averaged,

$$U = \frac{1}{hT}\int_0^T \int_0^h u(z,t)\mathrm{d}z\mathrm{d}t. \quad (1)$$

The depth-averaged cross (U)- and alongshore (V) velocity components are compared with the hourly averaged lowest em current meter and lowest ADCP bin (Fig. 12). The lowest bin of the ADCP is significantly correlated with the U and V with minimal bias. The lowest em current meter is also significantly correlated with V, but is less significantly correlated with U, owing to the influences of the bottom boundary layer of the dominant normally-

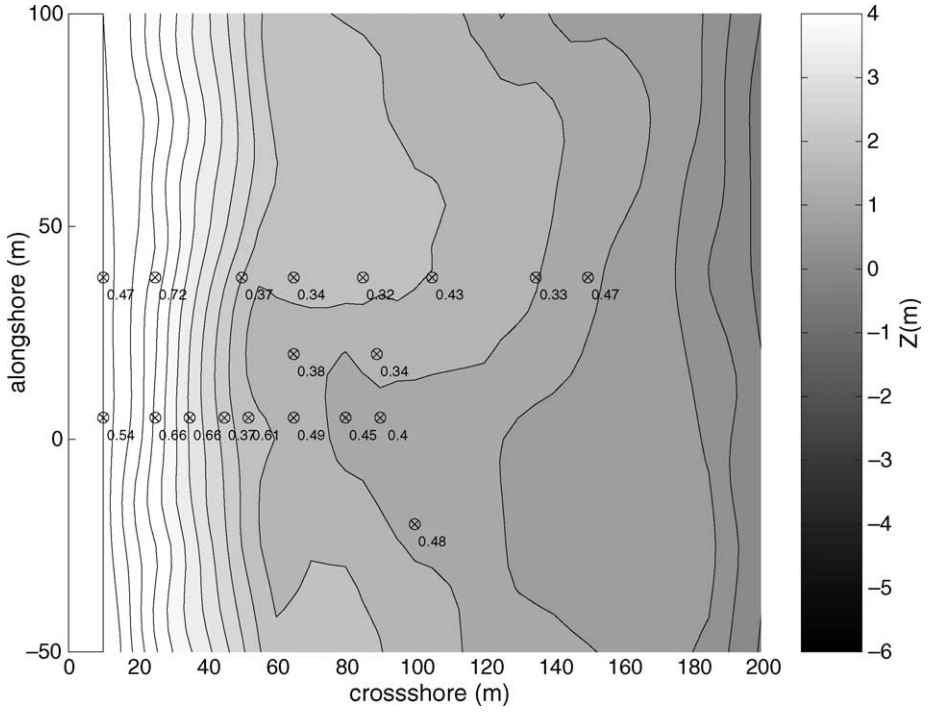

Fig. 11. Spatial distribution (⊗) of D_{50} overlayed on top of the bathymetric contours (color scale on the right) in the background.

incident waves. The assumption that the single-point em current meters is a valid representation of the depth-averaged flow appears reasonable.

Vertical velocity profiles were measured with a vertical array of 8 em current meters on the transverse bar. The flow on the transverse bar was shoreward over the water column and tidally modulated, with maximum shoreward currents occurring during low tides and during larger wave energy (Fig. 13). There was no seaward-directed return flow over the transverse bar, also referred to as undertow (Svendsen, 1984b) or bed return flow (Short, 1999), which is commonly observed for alongshore uniform beach profiles (Garcez Faria et al., 2000). The transverse bar flow is dominated by shoreward and alongshore currents, similar to the single-point measurements (Figs. 8–10). Zero mean flow occurred around high tides or during low wave energy. At high tides, waves generally break on the steep beachface inducing minimal alongshore variations in wave breaking. The rip channels drain the surf zone more efficiently due to a greater hydraulic radius of the rip channels compared with the transverse bars, where hydraulic radius is defined as the cross-sectional area divided by wetted perimeter of the channel (or transverse bar). Svendsen et al. (2000) found from model simulations that rip current circulation is a localized flow pattern and that if the rip spacing (λ_{rip})>(4–8)w_r (where w_r is the rip channel width) the neighboring rip currents are not influenced by each other. They also found that the two-dimensional bar return flow (undertow) was a function of rip channel spacing. For RIPEX, λ_{rip}/w_r was less than or equal to two, indicating that the rip currents are influenced by each other.

The vertical velocity profile within the rip channel was measured with the portable ADCP deployed on yeardays 101–102 (Fig. 14). Haas and Svendsen (2002) found in the laboratory that vertical velocity profiles were essentially uniform below the wave trough along the axis of a rip channel within the surf zone. Kennedy and Thomas (2004) used surface drifters in the same laboratory

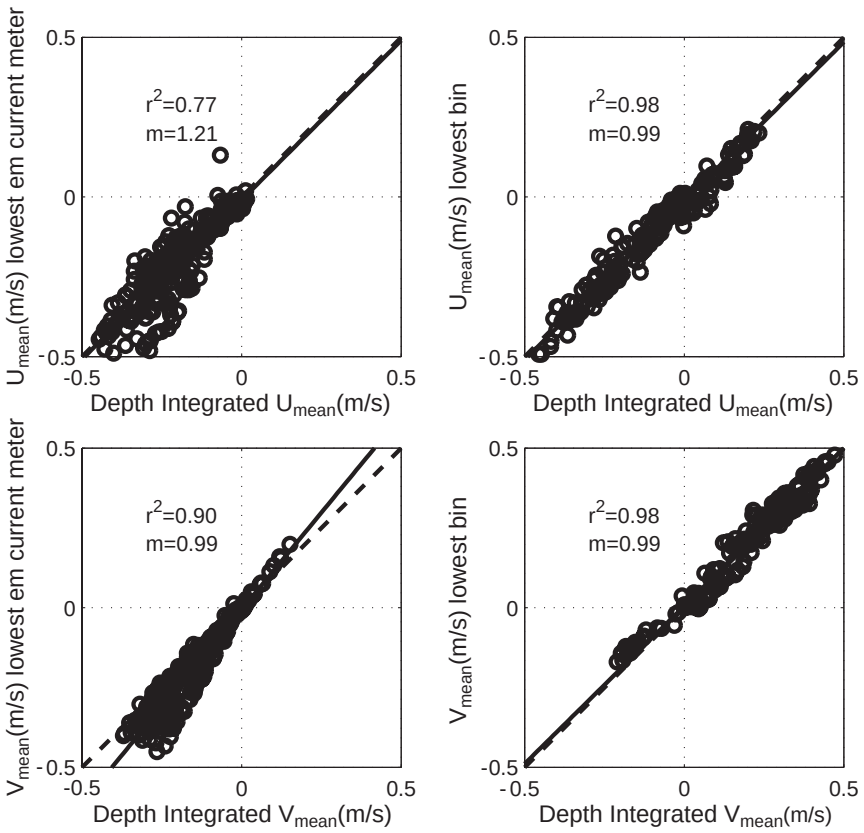

Fig. 12. Depth-averaged cross-shore (top) and alongshore (bottom) velocity measurements correlated with the lowest em current meter from the tower (left) and lowest bin from the aquadopp (right). The dashed line represents unity. m is the slope of line determined by the linear regression.

setting and their measurements suggest significant onshore flow contribution above the trough within the rip current owing to Stokes drift and the roller. This suggests significant shear over the vertical, in particular near the trough. The ADCP can measure velocities over the vertical including the crest-trough region. In an Eulerian measurement, the averaged-hourly flow decreases towards the surface as the bins within the trough to crest region are increasingly out of the water. In the absence of waves, the velocity profile would uniformly extend to the MSL, $z/h=1$. In the Eulerian reference frame, the presence of waves induces an onshore Stokes drift counter to the rip current at the surface, which results in a significant vertical shear in the crest-trough region (Fig. 15). The normalized Stokes drift, $\frac{E}{\rho C^2 H_{\mathrm{rms}}} \simeq 0.1$, is similar to the measured deficit at MSL. Therefore, the surface flow field is different than the underlying flow field, supported by drifter observations in the laboratory (Kennedy and Thomas, 2004) and field (Schmidt et al., 2003).

4.4. Tidal modulation

Changes in tidal elevation have been shown to modify the strength of rip current flow with the rip currents increasing to a relative maximum at low tidal elevations (Sonu, 1972; Aagaard et al., 1997; Brander, 1999; Brander and Short, 2001). Mean velocity magnitudes (over 90 min) were computed for two sensors (PUV9, PUV6) located within two different rip current channels (Fig. 1). The rip current velocities have a strong tidal modulation, with

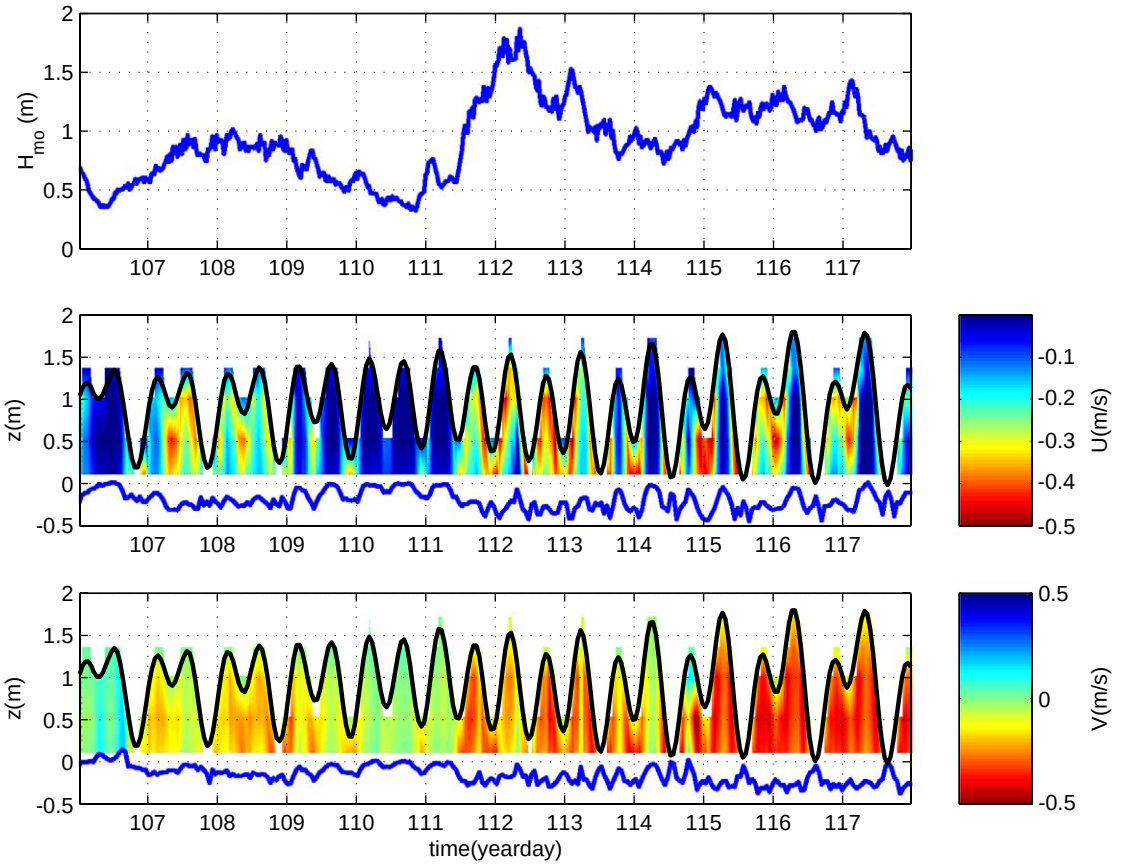

Fig. 13. (top) H_{mo} provided for comparison (middle) hourly mean cross-shore profiles (color scale on right) with depth-averaged velocities plotted beneath (Positive U is offshore), (bottom) hourly alongshore profiles (color scale on right) with depth integrated velocities plotted beneath (Positive V is north). The position of the tower is at the location of the MAST on Fig. 1.

increasing speeds occurring with decreasing tidal elevation (Fig. 16), consistent with previous field observations. Velocity magnitudes $\left(U_r = \sqrt{u^2 + v^2}\right)$ were computed as the sensors were relatively close to the feeder channels and the flow direction was not necessarily oriented offshore. The slight decrease in mean flow maxima at low tide are a result of the em currents being influenced by Stokes drift.

4.5. Dimensionless relationship

Rip current velocities increase with increase in wave heights, which can occur during high tide offsetting the effects of tidal modulation (Fig. 14). Thus, tidal elevation and wave forcing both are important factors that determine the flow speed within a rip channel. The rip current velocities increase with increasing sea-swell energy similar to observations by Shepard and Inman (1950).

Haller et al. (2002) and Dronen et al. (2002) in laboratory settings, computed the dimensionless rip current velocity (Froude Number) and found a relationship between dimensionless rip current velocity and normalized wave height,

$$\frac{U_r}{\sqrt{gh}} \sim \frac{H_o}{h}, \tag{2}$$

where U_r is the mean return flow, H_o is the deep water, significant wave height, and h is the local

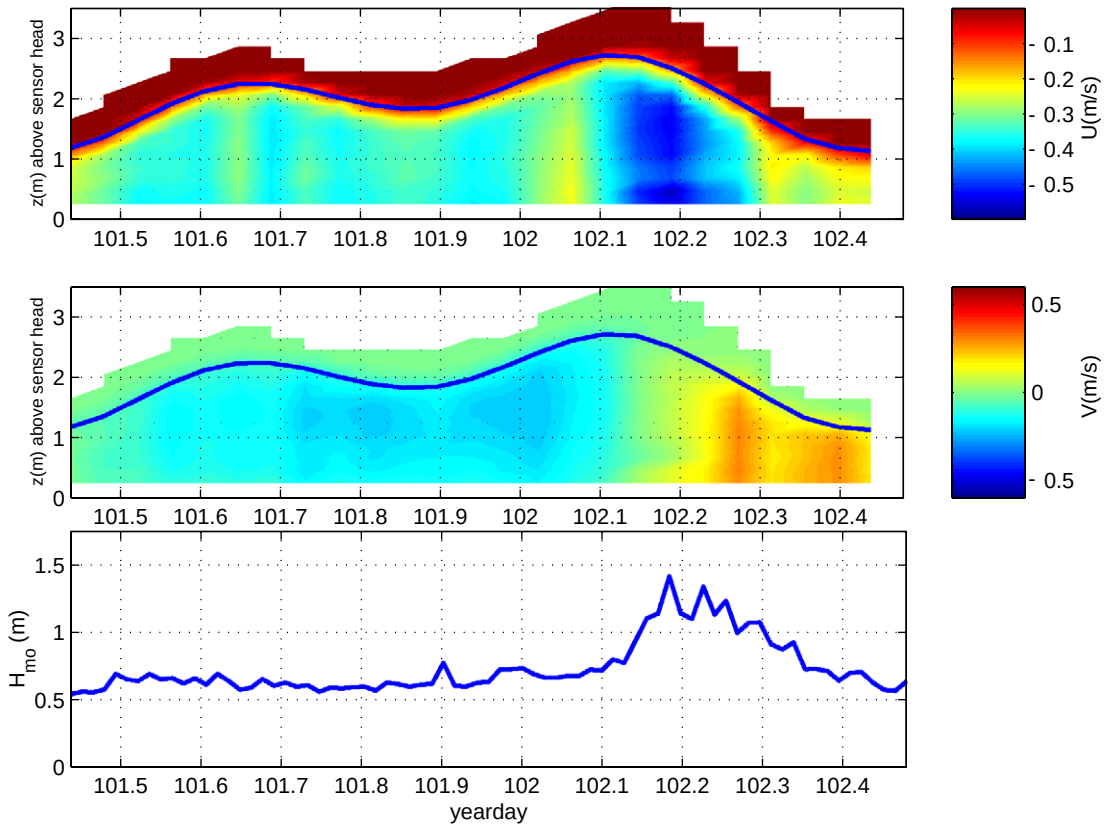

Fig. 14. Vertical distributions of cross-shore (top) and alongshore (middle) velocities within the rip current (color scale on right). Mean water level is indicated by the heavy line. (bottom) Significant wave height (H_{mo}) measured at the ADCP.

water depth over the transverse bar crest. Evaluating these parameters for 90 min mean speeds $\left(\sqrt{u^2+v^2}\right)$ for sensors (PUV4, 6, 9, 10) within the rip channel, an approximate linear relationship is found for $H_o/h_{bar}<1$, which is significantly correlated at the 95% confidence level (Fig. 17). For $H_o/h_{bar}>1$, the dimensionless return flow approaches a relative (qualitative) maximum. For $(H_o/h_{bar})>1$, the waves on the transverse bar become saturated (wave height is depth-limited due to wave breaking, $H/h \simeq 0.6$), which infers that pressure gradients and wave mass transport should not change. The relationship performs better for sensors located within the center of rip channel and farther offshore, which were influenced less by the feeder channels.

PUV10 was originally located within the rip channel, but as the rip channels slowly migrated downcoast, it became part of the transverse bar/feeder current system. PUV10 has the lowest apparent upper limit, due its proximity to the shoreline. This indicates that the velocity here achieves a maximum before sensors located deeper within the rip channels. PUV6 and PUV9 were located in nearly the same depth, though in different rip channels, and have a similar upper limit. PUV11 has a lower upper dimensionless return flow limit, as it was located slightly farther inshore than PUV6 and was less centered within the rip channel. The results for Dronen et al. (2002), indicate that their data began to approach an upper limit with a dimensionless return flow velocity of 0.6 in the proximity of $H_o/h_{bar}=1$. The dataset of Haller et al. (2002) does not appear to reach an upper limit, even though measurements occur at H_o/h_{bar} are approximately 3, which may be associated with the alongshore sloping basin (Haas et al., 2003).

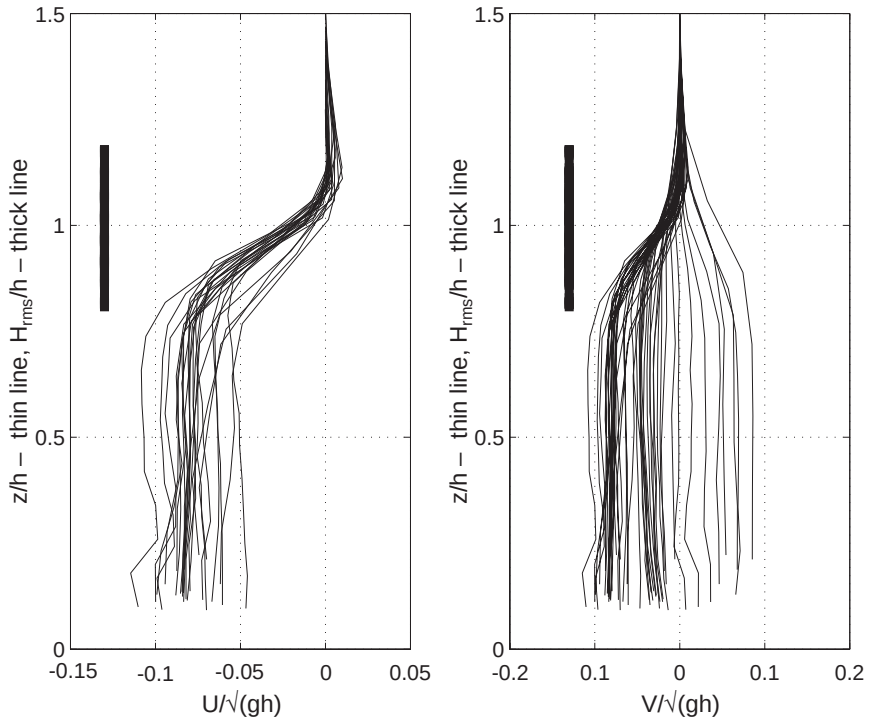

Fig. 15. Vertical distributions of cross-shore (left) and alongshore (right) velocities within the rip current. The mean water level is located at $z/h=1$. H_{rms} is indicated by the bold vertical line, representing the range of values, and indicates that most of the shear is in the crest-trough region.

The asymptotic limit will vary for different geometrical configurations, wave climate, and tidal elevation. Currently, there are not enough measurements of rip current flows under extreme conditions to accurately predict the asymptotic limit for a rip current system at various depths.

4.6. Wave-induced transport on a rip channel beach

Munk (1949) originally suggested that rip currents were formed by onshore wave mass transport and that this water piled up against the beach, which provided a hydraulic head for an offshore return flow (rip current). Aagaard et al. (1997) and Brander and Short (2001) used this simple kinematic (conceptual) model to explain observed velocities in the rip channel based on the continuity equation, in which the discharge out (Q_{out}) of the rip channel is equal to incoming wave-induced transport over the transverse bar (Q_{in}), computed by

$$Q_{out} = Q_{in} = (Q_{Stokes} + Q_{roller})\lambda_{rip}, \quad (3)$$

where

$$Q_{Stokes} = \frac{gH^2}{8C}, \quad (4)$$

$$Q_{roller} = \frac{0.9H^2}{T}, \quad (5)$$

where Q_{Stokes} is the second order Stokes drift, Q_{roller} is the transport due to the broken wave bore (Svendsen, 1984a,b), g is the gravitational acceleration, C is the wave phase speed, and λ_{rip} is rip channel spacing, and

$$Q_{out} = U_r A_r, \quad (6)$$

where U_r is the rip current velocity and A_r is the cross-sectional area, which was tidally modified. Aagaard et al. (1997) and Brander and Short (2001) found good agreement. However, for the measurements presented here based on the alongshore array, Q_{out} is biased high relative to Q_{in} (Eq. (3)) (Fig. 18). PUV6, 9, 10 were located relatively in the center of the channel (Fig. 1),

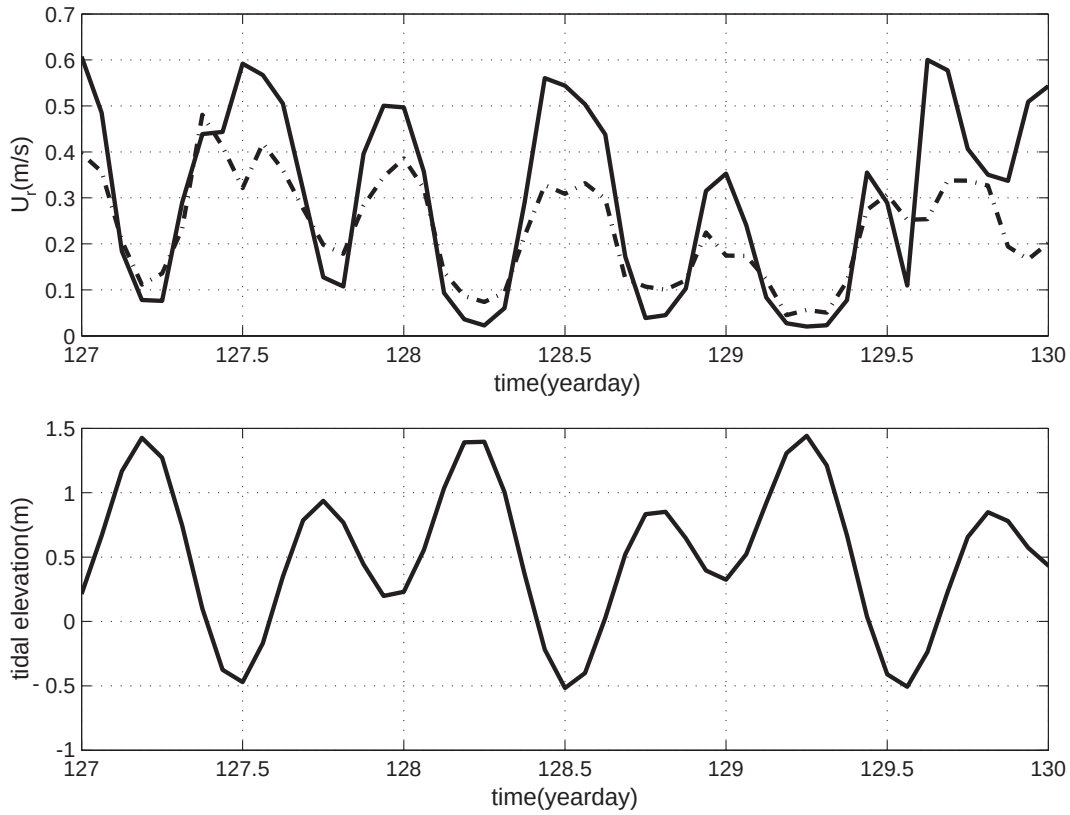

Fig. 16. (top) Tidal modulation of rip currents speeds (90 min averages) recorded within two different rip current channels for several days where the wave conditions were relatively constant; dashed line represents velocity magnitudes at PUV9, solid line at PUV6 within the rip channel. (bottom) Concurrent tidal elevation measured at PUV6 relative to MSL.

and since there was not a dense array across the channel, it is assumed that the velocity measurements are representative of the mean flow.

An inherent problem with applying the continuity equation equation expressed by Eq. (3) is that as the spacing of the rip channels become large, the rip current velocity can approach infinity (Kennedy and Thomas, 2004). Svendsen et al. (2000) determined that the mass transport returns as a two-dimensional bar return flow for increasing bar length and found that the total volume flux is independent of the bar length.

The configuration of RIPEX system has rip current circulation cells (Fig. 8) that are close together (λ_{rip}=125 m). In this case, the continuity Eq. (3) does not explain the seaward-directed flow within the rip channel, resulting in predictions that are biased high.

The continuity equation describes the kinematics, but not the dynamics. Additional flow contributions need to be included that are associated with nearshore radiation stress gradients due to differential breaking wave patterns, which have been neglected. In an Eulerian frame of reference, the shoreward Stokes mass transport occurs between the trough and crest region, and an additional flow contribution was measured below the trough (Eq. (1)) (Fig. 9). Therefore, Q_{in} is modified to include $Q_{Eulerian}$,

$$Q_{in} = (Q_{Eulerian} + Q_{Stokes} + Q_{roller})\lambda_{rip}, \quad (7)$$

and

$$Q_{out} = U_r A_r - Q_{Stokes}, \quad (8)$$

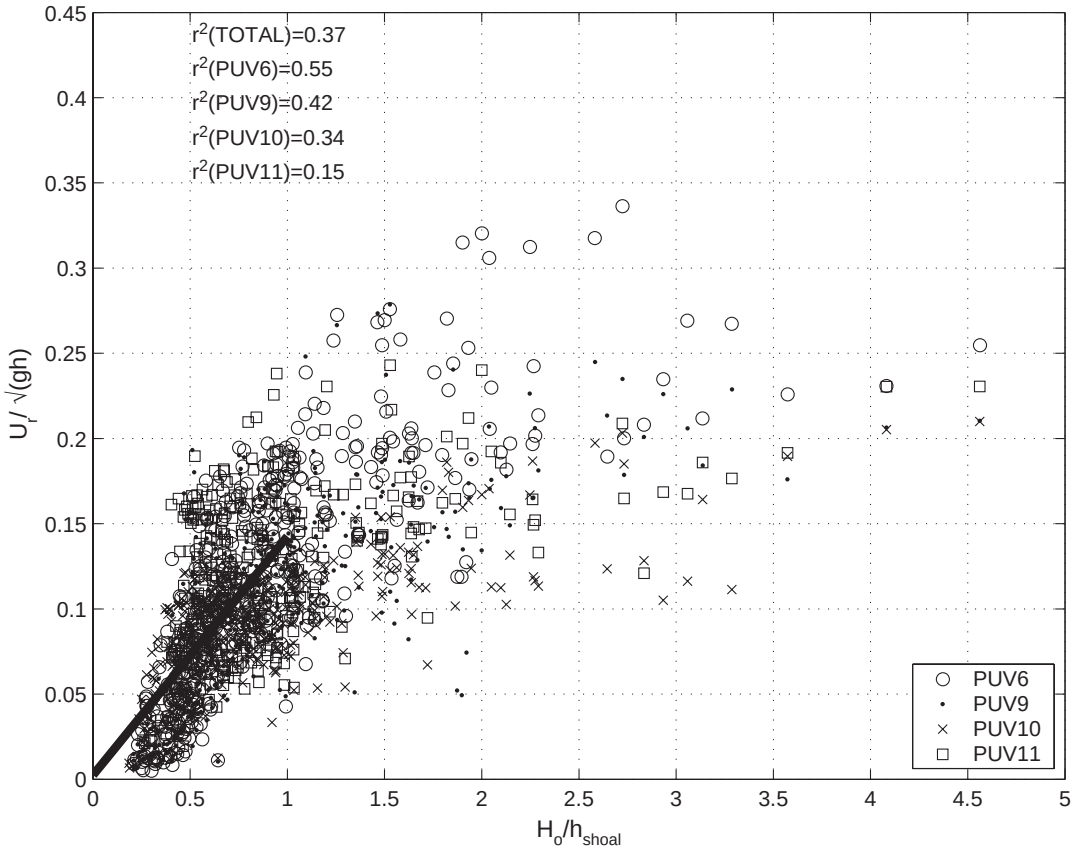

Fig. 17. Dimensionless return flow, U_r, as function of H_o/h_{bar} for 90 min mean rip current flows measured at PUV6,9,10,11 for yeardays 107–140. Solid line represents least-squares linear fit for all sensors, total and individual sensor r^2 are presented for $H_o/h_{bar} \leq 1$.

where $Q_{Eulerian} = U_{bar} h_{bar} \lambda_{bar}$ and U_{bar} is the measured transverse bar velocity (PUV1, 2). Including the Eulerian transport increases the total discharge over the transverse bar to approximately the same order of magnitude as Q_{out} (Fig. 18). There still is significant scatter amongst the data associated with using single point velocity measurements to represent the volume flux. Though the relationships are statistically significant for both conceptual models, including the $Q_{Eulerian}$ reduces the bias.

5. Summary

Rip current kinematics and beach morphodynamics were measured for 44 days at Sand City, Monterey Bay, CA obtained from 15 instruments composed of co-located velocity and pressure sensors, acoustic Doppler current profilers, and rapid kinematic GPS bathymetric mappings. The morphology consisted of a low-tide terrace incised with quasi-periodic rip channels, transverse bars system (Wright and Short, 1984). Offshore (17 m) wave heights and periods ranged 0.20–4.0 m and 5–20 s. The mean wave direction was consistently near 0° resulting in persistent rip channels, which evolved in response to the changing wave characteristics. Video images are found to be a good proxy for the rip channel bathymetry for wave heights less than 2 m. When the wave heights exceed 2 m, the rip channels are obscured by wave breaking, but flow measurements indicate strong, O (1m/s), rip currents were still present. It was found that there was an inverse relationship between

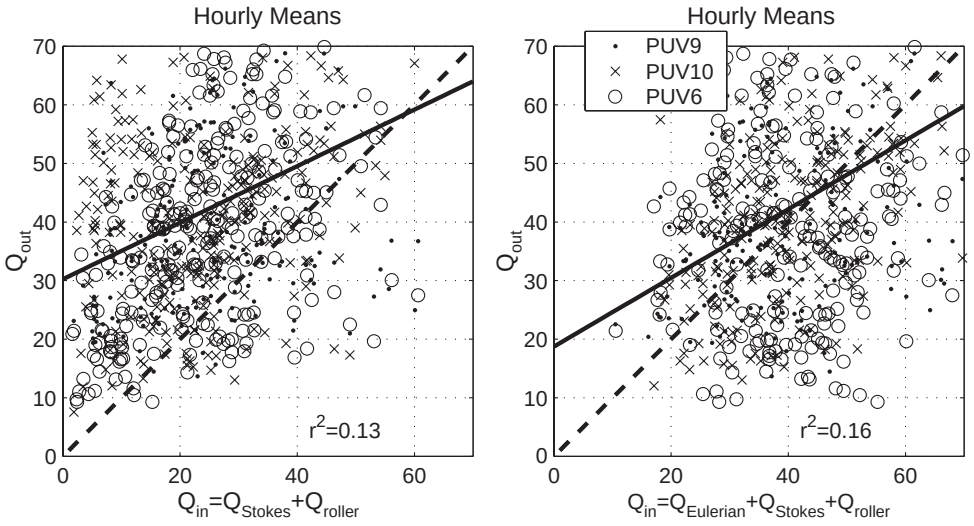

Fig. 18. Daily estimates of transverse bar (Q_{in}) and rip channel discharge (Q_{out}), which are both significantly correlated based on the large number of points.

erosional and accretional trends between the rip channels and the neighboring transverse bars, once the system reached equilibrium. The spatial distribution of sediments reflects the background rip current flow field.

The cellular circulation of rip currents was a persistent background flow, with predominantly shoreward flow on the transverse bars $P(U(\leq 0) \simeq 0.90)$ and seaward flow within the rip channels ($P\ (U \geq 0) \simeq 0.90$). The alongshore flows were equally-distributed or directionally-biased owing to the instrument location relative to the continuously evolving rip morphology. Vertical profiles illustrate that no seaward two dimensional return flow (undertow) was present on the transverse bar. Vertical profiles within the rip channel found large, near surface, vertical shear owing to the offshore flowing rip current encountering the onshore flowing Stokes drift. Single point measurements reasonably represented the depth averaged flow from bottom to MSL calculated from the vertical profiles within the surf zone. Temporal variations in mean rip current velocities were correlated with offshore sea-swell conditions and inversely related to tidal elevation. Non-dimensional rip current flows $\left(U_r/\sqrt{(gh)}\right)$ were significantly correlated with $H_o/h_{bar} < 1$ resulting in an $r^2 \sim 0.37$ for various instruments in the nearshore, similar to relationships found in laboratory measurement. However, an upper limit was found in the field measurements. Observations show that the onshore Eulerian transport over the bar and the onshore transport of waves within the rip channel should be accounted for in the continuity equation that were not previously included.

Acknowledgements

We extend our appreciation to the many folks who assisted in obtaining a great data set: Loraine Chial, Ron Cowen, Jason Engle, James Joyner, Gregory Miller, Tom Lippmann, Denis Morichon, Bruce Morris, Mark Orzech, Jennifer Short, Sidney Schofield, Jim Stockel, Charlotte Webb, Rob Wyland and volunteers from the Hopkins Marine Station (Stanford University) led by Mark Denny. We thank Tom Herbers and Paul Jessen for providing offshore buoy data. A special thanks to Edie Gallagher for leading the survey work. We thank Nathaniel Plant for the video rectification. The Steep Beach Experiment was funded by the Office of Naval Research (ONR), Coastal Sciences Program under contract N0001402WR20188 and data analysis by the National Science Foundation under contract OCE-01366882 and ONR. JM held a National Research Council-NPS Research Associate-

ship funded by the National Science Foundation under contract OCE-01366882 and ONR contract N0001402WR20188. Additional funding was provied to JM by the Florida Sea Grant Program. AR held a National Research Council-NPS Research Associateship funded by ONR. Additional funding for AR was provided by the Dutch National Science Foundation, contract DCB.5856. We appreciate the discussions with Graham Symonds. We thank the reviewers for their comments, which has improved the quality of the paper.

References

Aagaard, T., Greenwood, B., Nielsen, J., 1997. Mean currents and sediment transport in a rip channel. Mar. Geol. 140, 24–45.

Bowen, A.J., 1969. Rip currents: 1. Theoretical investigations. J. Geophys. Res. 74, 5467–5478.

Bowman, D., Arad, D., Rosen, D.S., Kit, E., Golbery, R., Slavicz, A., 1988a. Flow characteristics along the rip current system under low-energy conditions. Mar. Geol. 82, 149–167.

Bowman, D., Rosen, D.S., Kit, E., Arad, D., Slavicz, A., 1988b. Flow characteristics at the rip current neck under low-energy conditions. Mar. Geol. 79, 41–54.

Brander, R.W., 1999. Field observations on the morphodynamic evolution of low wave energy rip current system. Mar. Geol. 157, 199–217.

Brander, R.W., Short, A.D., 2000. Morphodynamics of a large-scale rip current system at Muriwai Beach, New Zealand. Mar. Geol. 165, 27–39.

Brander, R.W., Short, A.D., 2001. Flow kinematics of low-energy rip current systems. J. Coast. Res. 17:2, 468–481.

Cooke, D.O., 1970. The occurrence and geologic work of rip currents off southern California. Mar. Geol. 9, 173–186.

Dalrymple, R.A., 1978. Rip currents and their genesis. Summaries, 16th International Conference on Coastal Engineering, Conference Paper No 140.

Dronen, N., Karunarathna, H., Fredsoe, J., Sumer, B.M., Deigaard, R., 2002. An experimental study of rip channel flow. Coast. Eng. 45 (3–4), 223–238.

Engle, J., MacMahan, J., Thieke, R.J., Hanes, D.M., Dean, R.G., 2002. Formulation of a rip current predictive index using rescue data. Florida Shore and Beach Preservation Association National Conference.

Garcez Faria, A.F., Thornton, E.B., Lippmann, T.C., Stanton, T.P., 2000. Undertow over a barred beach. J. Geophys. Res. 105, 16999, 17010.

Haas, K.A., Svendsen, I.A., 2002. Laboratory measurements of the vertical structure of rip currents. J. Geophys. Res., 107.

Haas, K.A., Svendsen, I.A., Haller, M.C., Zhao, G., 2003. Quasi-three-dimensional modeling of rip current system. J. Geophys. Res., 108.

Haller, M.C., Dalrymple, R.A., Svendsen, I.A., 2002. Experimental study of nearshore dynamics on a barred beach with rip channels. J. Geophys. Res. 107 (14), 1–21.

Holt, R., 2003, MS thesis, Naval Postgraduate School.

Kennedy, A.B., Thomas, D., 2004. Drifter measurements in a laboratory rip current. J. Geophys. Res. 109, C08005.

Komar, P.D., 1971. Nearshore cell circulation of the formation of giant cusps. Geol. Soc. Amer. Bull. 82, 2643–2650.

Komar, P.D., 1998. Beach Processes and Sedimentation. Prentice Hall, London. 544 pp.

Lascody, R.L., 1998. East central Florida rip current program. National Weather Service In-House Report, p. 10.

Lippmann, T.C., Holman, R.A., 1990. The spatial and temporal variability of sand bar morphology. J. Geophys. Res. 95 (7), 11575–11590.

Luschine, J.B., 1991. A study of rip current drownings and weather related factors. Natl. Weather Dig., 13–19.

MacMahan, J., 2001. Hydrographic surveying from a personal watercraft. J. Surv. Eng. 127 (1).

MacMahan, J., Reniers, A.J.H.M., Thornton, E.B., Stanton, T., 2004. Infragravity rip current pulsations. J. Geophys. Res. 109, C01033.

MacMahan, J.H., Reniers, A.J.H.M., Thornton, E.B., Stanton, T.P., 2004. Surf zone eddies coupled with rip current morphology. J. Geophys. Res. 109, C07004.

Miller, G., 2001, MS thesis, University of Florida.

Munk, W.H., 1949. The solitary wave theory and application to surf problems. Ann. N.Y. Acad. Sci. 51 (3), 376–424.

Schmidt, W., Woodward, B., Millikan, K., Guza, R., Raubenheimer, B., Elgar, S., 2003. A GPS-tracked surf zone drifter. J. Atmos. Ocean. Technol. 20 (97), 1069–1075.

Shepard, F.P., Inman, D.L., 1950. Nearshore water circulation related to bottom topography and refraction. Trans.-Am. Geophys. Union 31, 196–212.

Sherman, D.J., Short, A.D., Takeda, I., 1993. Sediment mixing depth and bedform migration in rip channels. J. Coast. Res. 15, 39–48 (special issue).

Short, A.D., 1985. Rip current type, spacing and persistence, Narrabeen beach, Australia. Mar. Geol. 65, 47–71.

Short, A.D., 1999. Handbook of Beach and Shoreface Morphodynamics. John Wiley and Sons, p. 379.

Short, A.D., Hesp, P.A., 1982. Wave, beach and dune interactions in southwest Australia. Mar. Geol. 48, 259–284.

Short, A.D., Hogan, C.L., 1994. Rip currents and beach hazards, thier impact on public safety and implications for coastal mangement. In: Finkl, C.W. (Ed.), Coastal Hazards, Journal of Coastal Research, Special Issue, vol. 12, pp. 197–209.

Sonu, C.J., 1972. Field observations of nearshore circulation and meandering currents. J. Geophys. Res. 77, 3232–3247.

Svendsen, I.A., 1984a. Wave heights and set-up in a surf zone, Coast. Eng., 8, 303, 329.

Svendsen, I.A., 1984b. Mass flux and undertow in a surf zone, Coast. Eng. 8, 347, 365.

Svendsen, I.A., Haas, K.A., Zhao, Q., 2000. Analysis of rip current systems. In: Edge, B.L. (Ed.), Coastal Engineering 2000. Proceedings of 27th International Conference. Am. Soc. Civ. Eng., New York, pp. 1127–1140.

Thornton, E.B., Swayne, J.L., Dingler, J.R., 1998. Small-scale morphologyrealted to waves and currents across the surf zone. Mar. Geol. 145, 173–196.

Weltmer, M., 2003. Bedform evolution and sediment transport under breaking waves, MS thesis, Naval Postgraduate School, p. 86.

Wright, L.D., Short, A.D., 1984. Morhodynamic variability of surf zones and beaches: a synthesis. Mar. Geol. 70, 251–285.

Wright, L.D., Guza, R.T., Short, A.D., 1982. Dynamics of a high energy dissipative surf zone. Mar. Geol. 45, 41–62.